In vitro Disposition Profiling of Heterocyclic compounds

Janneke Keemink[a], Benjamin Wuyts[a], Johan Nicolaï[a], Steven De Jonghe[b,c], Alessandro Stella[b], Piet Herdewijn[b], Patrick Augustijns[a], Pieter Annaert[a*]

[a]Drug Delivery and Disposition, KU Leuven Department of Pharmaceutical and Pharmacological Sciences, Belgium.

[b]Laboratory for Medicinal Chemistry, Rega Institute, KU Leuven, Belgium.

Address: Rega Institute, Laboratory of Medicinal Chemistry, Minderbroedersstraat 10, 3000 Leuven, Belgium. tel +32 16 337367 fax +32 16 337340

[c]Interface Valorisation Platform (IVAP), Laboratory of Medicinal Chemistry, KU Leuven Belgium.

Address: IVAP, KU Leuven, Kapucijnenvoer 33, 8th Floor, 3000 Leuven, Belgium. tel. +32 16 3 32770 fax +32 16 3 32773

*Corresponding author:

Pieter Annaert

Drug Delivery and Disposition, University of Leuven, Gasthuisberg O&N 2 – Herestraat 49, box 921, 3000 Leuven, Belgium;

Tel: +32 16 330303; Fax: +32 16 330305

Pieter.annaert@pharm.kuleuven.be

ABSTRACT

Compound libraries that are screened for biological activity commonly contain heterocycles. Besides potency, drug-like properties need to be evaluated to ensure *in vivo* efficacy of test compounds. In this context, we determined hepatic and intestinal disposition profiles for 19 heterocyclic compounds.

All studied compounds showed rapid uptake in suspended rat hepatocytes, whereas metabolism was poor and the rate-limiting step in hepatic elimination. *In vitro* assays demonstrated a relatively low solubility and high intestinal permeability. Based on these *in vitro* data, heterocycles were categorized in the biopharmaceutics classification system (BCS) and the biopharmaceutics drug disposition classification system (BDDCS) to predict disposition characteristics before clinical data are available. Our findings emphasized the importance to use hepatocytes in addition to microsomes to study metabolism, since the latter lack non-microsomal enzymes and cellular context. Moreover, intracellular exposure should be considered to gain insight in the relevant fraction of the compound available at the enzymatic site. Finally, the study reveals discrepancies associated with the classification of heterocycles in BCS versus BDDCS. These probably originate from the binary character of both systems.

KEY WORDS: heterocycles, hepatic drug disposition, intestinal drug disposition, ADMET, biopharmaceutics drug disposition classification system (BDDCS)

ABBREVIATIONS: ABT, 1-aminobenzotriazole; ADMET, absorption distribution metabolism excretion toxicity; BCS, biopharmaceutics classification system; BDDCS, biopharmaceutics drug disposition classification system; $Cl_{int,basolateral}$, intrinsic basolateral clearance; $Cl_{int,canalicular}$, intrinsic canalicular clearance; $Cl_{int,met,hep}$, intrinsic metabolic clearance determined in hepatocytes; $Cl_{int,met,mic}$, intrinsic metabolic clearance determined in microsomes; $Cl_{int,uptake}$, intrinsic uptake clearance; $Cl_{passive}$, passive uptake hepatocytes; $Cl_{renal,filtration}$ renal clearance through glomerular filtration; CYP, cytochrome P450; DMEM, Dulbecco's modified Eagle's medium; DMSO, dimethyl sulfoxide; ER, extraction ratio; FaSSIF, fasted state simulated intestinal fluid; FBS, fetal bovine serum; fu, unbound fraction; $fu_{,hep}$, unbound fraction in hepatocyte incubations; $fu_{,mic}$, unbound fraction in microsomal incubations; GFR glomerular filtration rat; HB_a, hydrogen bond acceptor; HB_d, hydrogen bond donor; HBSS, hanks' balanced salt solution; HEPES, 4-(2-hydroxyethyl)-1-piperazineethanesulfonic acid; hOATP, human organic anion transporting polypeptide; KHB, Krebs Henseleit buffer; Km, Michaelis-Menten constant; Km_{enzyme}, intracellular unbound enzymatic Km, $Km_{hep,u,ex}$, unbound extracellular Km for metabolism; $Kp_{u,u}$, ratio of the intracellular to extracellular unbound concentration; L-15, Leibovitz; LogD, distribution coefficient; NADPH, nicotinamide adenine dinucleotide phosphate; NCE, new chemical entity; $P_{app,}$ apparent permeability coefficient; PBS, phosphate buffered saline; pKa, acid dissociation constant; PSA, polar surface area; RLM, rat liver microsomes; SCRH, sandwich-cultured rat hepatocytes; SDS, sodium dodecyl sulfate; SRH, suspended rat hepatocytes; TPGS1000, D-α-tocopheryl polyethylene glycol 1000 succinate; WEM, Williams' E medium; WST-1, water soluble tetrazolium-1

1. INTRODUCTION

Many drug discovery programs start with the screening of large compound libraries (either corporate or commercially available compound collections) in an appropriate target- or cell-based assay. The selection of 'hit' compounds is usually based on the selective affinity of compounds for a target protein or the potency of the compounds in a phenotypic assay. In addition, it is also important that drug candidates possess the appropriate physicochemical properties, such that a safe delivery at the target site can be ensured to obtain efficacy *in vivo* and that the compound ultimately can be developed as a drug. This implies that a balance needs to be found between the biological activities and drug-like properties of the compound. Drug-like molecules are defined as compounds with acceptable absorption, distribution, metabolism and excretion properties, along with an acceptable toxicity (ADMET) (Fan and de Lannoy, 2014). Therefore, it is of utmost importance to evaluate drug-like properties in an early stage of drug-development to prevent high attrition rates due to unacceptable pharmacokinetics in a later stage (Wang and Urban, 2004).

In silico determination of various physicochemical properties, such as the distribution coefficient (LogD) and the polar surface area (PSA) allow the rapid estimation of ADMET properties and have been very popular among medicinal chemists as they are easy to calculate (Lipinski et al., 2001). However, these predictions are not always consistent with experimental observations, indicating that application of appropriate *in vitro* models to study drug disposition is desirable. Among ADMET properties, hepatic drug clearance is one of the most important features to be predicted (Di et al., 2013). Over the past few decades, hepatic clearance has often been estimated using liver microsomes (Chiba et al., 2009; Obach, 1999). However, limitations of this *in vitro* model are the lack of non-microsomal enzymes and cellular context. Therefore, more biorelevant experimental models should be implemented to obtain insight in all processes underlying drug disposition and clearance. To predict oral drug absorption, intestinal solubility and permeability are commonly evaluated. Pre-clinical data regarding solubility, permeability and metabolism have previously been used to predict intestinal drug absorption and

overall drug disposition based on the biopharmaceutics classification system (BCS) and biopharmaceutics drug disposition classification system (BDDCS) (Larregieu and Benet, 2014). However, both systems require information regarding solubility based on the highest administered dose thus limiting the evaluation of new compound collections using these classifications.

Traditional compound collections used for screening purposes consist of low molecular weight heterocycles, usually based on one or more (hetero) aromatic ring structures. In addition, there is a strong interest in the synthesis and biological evaluation of novel heterocycles as potential therapeutic agents (Jang et al., 2011). Therefore, a series of heterocycles synthesized during a drug discovery project (Figure 1) was presently used to evaluate applicability of different non-clinical models predicting ADMET properties. Since the fraction of the compound reaching the systemic circulation after oral administration is mainly influenced by processes occurring in the liver and intestine, this profiling study focused on the prediction of the hepatic and intestinal disposition. The information acquired from *in vitro* models was used to classify the heterocycles according to the BCS and BDDCS to predict drug disposition characteristics solely based on *in vitro* data.

2. MATERIALS & METHODS

2.1. Chemicals

The heterocycles were synthesized at the Laboratory of Medicinal Chemistry (Interface Valorisation Platform, IVAP, Sint-Rafaël, KU Leuven). Hanks' balanced salt solution (HBSS), Williams' E medium (WEM), Dulbecco's modified Eagle's medium (DMEM), phosphate buffered saline (PBS), penicillin/streptomycin (10,000 IU/mL, 10,000 µg/mL), nonessential amino acid medium (100x), L-glutamine, fetal bovine serum (FBS) and 4-(2-hydroxyethyl)-1-piperazineethanesulfonic acid (HEPES) were obtained from Lonza (Westburg, The Netherlands). Leibovitz (L-15) medium was acquired from Invitrogen (Carlsbad, CA). Simulated intestinal fluid (SIF) powder was purchased from Biorelevant (Croydon, UK). D-α-tocopheryl polyethylene glycol 1000 succinate (TPGS1000) was obtained from Eastman Chemical Company (Kingsport, TN), acetic acid from Chem-lab (Zedelgem, Belgium). GF120918 (elacridar) was provided by GSK (London, UK). Water was purified with a Maxima system (Elga Ltd., High Wycombe Bucks, UK). Dimethyl sulfoxide (DMSO) and Triton X-100 were obtained from Acros Organics (Geel, Belgium), sodium dodecyl sulfate (SDS) and sodium hydroxide pellets from Merck (Darmstadt, Germany). Sodium acetate trihydrate, methanol and acetonitrile were purchased from VWR International (Leuven, Belgium), cell proliferation reagent water soluble tetrazolium-1 (WST-1) from Roche (Mannheim, Germany). Indinavir was donated by Hetero Drugs Ltd. (Hyderabad, India). All other chemicals were purchased from Sigma-Aldrich (St Louis, MO).

2.2. *In silico* profiling

Marvin Sketch was used to determine key physicochemical properties: hydrogen bond acceptors (HB_a), hydrogen bond donors (HB_d), rotatable bonds (RB), LogD (pH 7.4), PSA and acid dissociation constant (pKa). The liver-to-blood partition coefficients ($K_{liver:blood}$) were calculated according to Paixão et al. Descriptors, used to calculated $K_{liver:blood}$, were obtained with ALOGPS 2.1 program and E-Dragon 1.0 software using SMILES converted to the 3D representation of the molecule with CORINA (Paixão et al.,

2014). Human organic anion transporting polypeptide (hOATP) 1B-inhibition potential was predicted using a proteochemometrics-based *in silico* model (De Bruyn et al., 2013).

2.3. Hepatic disposition profiling

2.3.1. Hepatocyte isolation

Hepatocytes were isolated from male Wistar rats (175-200 g) with a two-step collagenase perfusion as described previously (Annaert et al., 2001). Approval for the experiments was granted by the Institutional Ethical Committee for Animal Experimentation of the KU Leuven. After isolation, cells were centrifuged (50 *g*) for 3 min at 4°C and the pellet was resuspended in Krebs Henseleit buffer (KHB; 130 mM NaCl, 5.17 mM KCl, 1.2 mM $CaCl_2$, 1.2 mM $MgCl_2$, 12.5 mM HEPES, 11.1 mM glucose, 5 mM sodium pyruvate, pH 7.4), L-15 medium supplemented with 4 mM L-glutamine or seeding medium (WEM containing 2 mM L-glutamine, 100 IU/mL penicillin, 100 µg/mL streptomycin, 5 % FBS, 4 mg/L insulin and 1 µM dexamethasone). Viability was determined using the trypan blue exclusion method and was always higher than 85 %.

2.3.2. *In vitro* intrinsic uptake clearance in suspended rat hepatocytes

Experiments were conducted as described previously (De Bruyn, Fattah, *et al.*, 2011). Briefly, suspended rat hepatocytes (SRH) ($2x10^6$ cells/mL) in KHB were pre-warmed at 37°C (500 µL). The incubation was initiated by adding 500 µL of a pre-warmed double-concentrated heterocycle solution (final concentration 8 µM). After 1 min, aliquots of 200 µL were transferred in triplicate to ice-cold microcentrifuge tubes (1.5 mL), containing 700 µL of an oil mixture (density 1.015; a mixture of silicone oil and mineral oil) above 300 µL of 8 % NaCl solution. Tubes were centrifuged at 14,000 rpm for 2 min and frozen on dry ice. After freezing, the tube bottoms were cut and the cell lysate was solubilized in 300 µL methanol/water (70/30). Experiments were also performed at 4°C to determine nonsaturable uptake. Net uptake values were obtained by subtracting uptake in rat hepatocytes at 4°C from total uptake at 37°C. Subsequently, active, passive and total uptake clearance values ($Cl_{int,uptake}$; µl/min/million cells) were determined by dividing the net uptake, passive uptake or total uptake

(pmol/min/million cells) by the substrate concentration. Finally, $Cl_{int,uptake}$ was converted from µL/min/million cells to mL/min/kg bodyweight using the scaling factors 120 million cells/g liver and 40 g liver/kg body weight.

2.3.3. *In vitro* intrinsic metabolic clearance in suspended rat hepatocytes

Experiments were performed as described previously (Wuyts et al., 2013). Briefly, the incubation mixture consisted of the SRH (1x10^6 cells/mL) and heterocyclic compound (0.5-100 µM) in the presence or absence of 1-aminobenzotriazole (ABT; 1 mM) in L-15 medium supplemented with 4 mM L-glutamine (500 µL). At 0, 45 and 120 min, aliquots (150 µL) were taken and added to methanol (300 µL). Verapamil metabolism was determined as a positive control and incubations without cells were used as negative control.

In vitro hepatic metabolism of the compounds was assessed with the '*in vitro* half-life ($t_{1/2}$) method' (Obach, 1999) using scaling factors (Chiba et al., 1997). Intrinsic metabolic clearance obtained in hepatocytes ($Cl_{int,met,hep}$) was determined using the following equation:

$$Cl_{int,met,hep} = \frac{0{,}693}{t_{1/2}} \times \frac{incubation\ volume}{million\ cells} \times \frac{120\ million\ cells}{g\ liver} \times \frac{40\ g\ liver}{kg\ bodyweight}$$

(Equation 1)

For compound **1210,** Michaelis-Menten parameters regarding the metabolic disappearance were determined by non-linear regression analysis in R (version i386 2.15.3).

2.3.4. *In vitro* intrinsic metabolic clearance in rat liver microsomes

Rat liver microsomes (RLM) were prepared according to in-house procedures (Nicolaï et al., 2015). Microsomal incubations were performed at 37°C and 350 rpm (Thermomixer, Eppendorf AG, Hamburg, Germany). The incubation mixture consisted of RLM (0.5 mg/mL) and heterocyclic compound (0.5-100 µM) diluted in microsomal buffer (phosphate buffer (100 mM) containing $MgCl_2$ (3 mM) pH 7.4). After a pre-incubation of 10 min, nicotinamide adenine dinucleotide phosphate (NADPH) (1 mM) and

glucose-6-phosphate (3 mM) were added to initiate the reaction. Reactions were terminated by taking samples (75 µL) at 0, 10, 20 and 30 min and adding them to acetonitrile (75 µL).

In vitro hepatic metabolism of the compounds was assessed as described previously with the '*in vitro* $t_{1/2}$ method'. Intrinsic metabolic clearance obtained in microsomes ($Cl_{int,met,mic}$) was determined as follows:

$$Cl_{int,met,mic} = \frac{0{,}693}{t_{1/2}} \times \frac{incubation\ volume}{mg\ microsomes} \times \frac{46\ mg\ microsomes}{g\ liver} \times \frac{40\ g\ liver}{kg\ body\ weight}$$

(Equation 2)

For compound **1210** Michaelis-Menten parameters for the metabolic disappearance were determined by non-linear regression analysis in R (version i386 2.15.3).

2.3.5. Determination of unbound fraction in plasma and microsomal binding

The unbound fraction in plasma (fu) was determined for the heterocycles with equilibrium dialysis in the HTD96b setup from HTDialysis, LLC (Gales Ferry, CT, US). Pooled rat plasma (n=5) containing heterocyclic compound (8 µM) and PBS were added to the donor and acceptor compartment, respectively to determine plasma protein binding. For the microsomal binding, 0.5 mg/mL RLM in microsomal buffer containing heterocyclic compound (8 µM) was added to the donor compartment and microsomal buffer to the acceptor compartment. Samples (n=3) of both compartments were taken after a 6 h incubation at 37°C. The fu was determined using the following equation:

$$fu = \frac{[Compound]_{acceptor}}{[Compound]_{donor}}$$

(Equation 3)

2.3.6. Ratio of the intracellular to extracellular unbound concentration.

The ratio of the intracellular to extracellular unbound concentration ($Kp_{u,u}$) was determined according to Nicolaï et al. (Nicolaï et al., 2015). An apparent Michaelis constant (Km) was determined in hepatocytes (Km_{hep}) since metabolic enzymes reside inside hepatocytes. As only the unbound fraction (fu_{hep}) will be able to enter hepatocytes, the unbound extracellular Km ($Km_{hep,u,ex}$) was determined:

$$Km_{hep} \times fu_{hep} = Km_{hep,u,ex}$$

(Equation 4)

In RLM, cytochrome P450 (CYP)-mediated metabolism is measured without restriction regarding membrane permeability. Therefore, intracellular unbound enzymatic Km (Km_{enzyme}) could be determined based on Km determined in microsomes (Km_{mic}) and the unbound fraction in microsomal incubations (fu_{mic}) because these enzymes are assumed to retain affinity for specific compounds (Nicolaï et al., 2015). Km_{enzyme} was determined as follows:

$$Km_{mic} \times fu_{mic} = Km_{enzyme}$$

(Equation 5)

Consequently, in case of CYP-mediated metabolism, $Kp_{u,u}$ can be calculated:

$$\frac{Km_{enzyme}}{Km_{hep,u,ex}} = Kp_{u,u}$$

(Equation 6)

2.3.7. Canalicular and basolateral efflux in rat hepatocytes

Canalicular and basolateral efflux were assessed in sandwich-cultured rat hepatocytes (SCRH). SCRH were cultured as described previously (Wuyts et al., 2013). Briefly, freshly-isolated hepatocytes were seeded on collagen coated 24-well plates at a density of 0.5 x 10^6 cells/well in seeding medium. Cells were allowed to attach for 1-2 h, after which the medium was aspirated to remove unattached cells. Cells were overlaid with collagen and, after one hour, seeding medium was added onto the SCRH.

213 Culture medium was replaced daily (WEM containing 2 mM L-glutamine, 100 IU/mL penicillin, 100
214 µg/mL streptomycin, 1 % (v/v) ITS^{TM} + Premix and 0.1 µM dexamethasone).

215 On day 4, SCRH were rinsed twice and pre-incubated for 10 min with standard buffer (HBSS containing
216 10 mM HEPES; pH 7.4; 37°C). Subsequently, hepatocytes were loaded with representative compound
217 **1269** (8 µM) in standard buffer for 15 min. Wells were washed three times and part of the cells were
218 lysed with methanol/water (70/30) to determine accumulation after loading. Additionally, fresh
219 standard or Ca^{++}/Mg^{++}-free-buffer (Ca^{++}/Mg^{++}-free HBSS containing 10 mM HEPES and 1 mM EGTA; pH
220 7.4; 37°C) was added to the remaining wells. Samples of the buffer were taken after 15 min. Protein
221 content was determined in three representative wells using a BCA Protein assay kit (Pierce Chemical,
222 Rockford, Illinois).

223 Canalicular efflux was determined by subtracting substrate efflux in standard buffer (tight junctions
224 intact: efflux across basolateral membrane) from substrate efflux in Ca^{++}/Mg^{++}-free-buffer (tight
225 junctions disrupted: efflux across both basolateral and canalicular membrane). Basolateral efflux was
226 measured in standard buffer samples. Efflux was expressed as pmol/mg protein.

227 *In vitro* intrinsic canalicular ($Cl_{int,canalicular}$) and basolateral clearance ($Cl_{int,basolateral}$) were determined as
228 follows (Nakakariya et al., 2012):

229 $$Cl_{int,canalicular}\ or\ Cl_{int,basolateral} = \frac{Canalicular\ or\ Basolateral\ efflux}{Incubation\ time\ *\ C_{hep}}$$

230 (Equation 7)

231 $$C_{hep} = \frac{Accumulation\ in\ cells\ after\ loading}{Intracellular\ volume}$$

232 (Equation 8)

233 where efflux and accumulation in cells after loading were in pmol/mg protein, C_{hep} was the
234 concentration in hepatocytes and total intracellular volume was 5.2 µL/mg protein. $Cl_{int,canalicular}$ and

$Cl_{int,basolateral}$ were converted from µL/min/mg protein to mL/min/kg bodyweight using the scaling factors 200 mg protein/g liver and 40 g liver/kg body weight.

2.3.8. Metabolic site prediction

Metabolic sites of the heterocycle structures were predicted with MetaPrint2d (University of Cambrige) (http://www-metaprint2d.ch.cam.ac.uk/). The most frequently reported sites of metabolism are indicated by comparing the compounds with a database of structures with known metabolic patterns. Subsequently, the normalized occurrence ratio (NOR) is determined.

2.3.9. *In vitro – in vivo* extrapolation (IVIVE) of hepatic clearance

To evaluate the rate-limiting step in the overall hepatic elimination, the *in vivo* clearance of the heterocycles was predicted based on uptake data only ($Cl_{H,uptake}$), metabolism data only ($Cl_{H,met}$) or a combination of both (Cl_H). Therefore, previously determined intrinsic clearance values were converted to the hepatic *in vivo* clearance values with the well-stirred model (Webborn et al., 2007):

$$Cl_{H,uptake} = \frac{Q_H \cdot f_u \cdot (Cl_{int,uptake} + Cl_{passive})}{Q_H + f_u \cdot (Cl_{int,uptake} + Cl_{passive})}$$

(Equation 9)

$$Cl_{H,met} = \frac{Q_H \cdot f_u \cdot Cl_{int,met,hep}}{Q_H + f_u \cdot Cl_{int,met,hep}}$$

(Equation 10)

$$Cl_H = \frac{Q_H \cdot f_u \cdot Cl_{int,met,hep} \cdot (Cl_{int,uptake} + Cl_{passive})}{Q_H \cdot (Cl_{int,uptake} + Cl_{passive}) + ((Cl_{int,uptake} + Cl_{passive}) \cdot f_u \cdot Cl_{int,met,hep})}$$

(Equation 11)

where Q_H is the hepatic plasma flow (28.3 mL/min/kg) in rat, fu is the unbound fraction in plasma, Cl_{int} is the *in vitro* intrinsic clearance and $Cl_{passive}$ is the passive uptake in hepatocytes (4°C). Finally extraction ratios (ER) were determined (ER = Cl_H/Q_H). The ER describes the efficiency of the hepatic drug

elimination process; ER values between 0-0.3 reflect poor elimination, 0.3-0.7 intermediate elimination and 0.7-1 extensive elimination (Wuyts et al., 2013).

2.3.10. Hepatotoxicity

To determine hepatotoxicity, compound (5 or 50 µM) in culture medium was added onto SCRH one day after seeding. The urea assay was performed after 6, 48 and 72 h to evaluate cellular integrity and biochemical functionality (Chatterjee et al., 2014). Briefly, cells were rinsed twice with standard buffer followed by a pre-incubation for 10 min at 37°C. Subsequently, hepatocytes were loaded with incubation buffer (standard buffer containing 2 mM L-glutamine, 10 mM ammonium chloride and 3 mM ornithine) and incubated for 1 h at 37°C. Aliquots of the incubation buffer were taken and mixed with color reagent. The intensity of the color was measured spectrophotometrically at 525 nm.

2.4. Intestinal disposition profiling

2.4.1. Intraluminal solubility

The solubility of the compounds was determined in biorelevant fasted state simulated intestinal fluid (FaSSIF), possessing mixed micelles of taurocholate and lecithin. FaSSIF which was prepared by dissolving 2.24 mg/mL SIF powder in a phosphate buffer, blank FaSSIF (3.95 mg/mL $NaH_2PO_4.H_2O$, 6.19 mg/mL NaCl, 0.42 mg/mL NaOH, pH 6.5), according to the manufacturer's preparation protocol. The thermodynamic solubility was determined as described previously (Wuyts et al., 2013). Briefly, an excess of compound was added to FaSSIF (0.5 mg/300 µL). This suspension was shaken for 24 h at 175 rpm and 37°C (KS 4000i Control incubator shaker, Staufen, Germany) and centrifuged at 20,817 *g* for 15 min (5804 Centrifuge, Eppendorf, Hamburg, Germany) to remove undissolved drug. The supernatant was analyzed. **1351** and **1366** were excluded from further experiments due to extremely low solubility and chemical instability at 37°C, respectively.

2.4.2. Intestinal permeability

Intestinal permeability was determined as described previously (Wuyts et al., 2013). Briefly, Caco-2 cells were grown in DMEM supplemented with 10 % FBS, 1 % nonessential amino acid, 100 IU/mL penicillin and 100 µg/mL streptomycin at 37°C, in a humidified atmosphere with 5% CO_2. Cells were seeded at a density of 90,000 cells/cm^2 on Costar Transwell membrane inserts (3 µm pore diameter, 12 mm diameter; Corning Inc., Corning, NY) and were used in transport studies 17 to 18 days after seeding. Transport medium (HBSS supplemented with 25 mM glucose and 10 mM HEPES at pH 7.4) containing 0.2 % TPGS1000 was used in the basolateral compartment to create sink conditions and solubilize the drugs. The experiment was initiated by adding FaSSIF (pH 6.5) containing the heterocycles (10-100 µM) in absence or presence of P-gp-inhibitor GF120918 (4 µM), to the apical compartment. Samples were shaken at 300 rpm for 1h at 37°C (Thermostar, BMG Labtech, Offenburg, Germany).

The apparent permeability coefficient (P_{app}) was calculated according to the following equation:

$$P_{app} = \frac{\Delta Q}{\Delta t} \times \frac{1}{A * C_{donor}} \quad \text{(equation 12)}$$

where Q is the cumulative amount of drug appearing in the acceptor compartment, A is the surface area of the Transwell membrane (1.13 cm^2), and C_{donor} is the initial drug concentration in the apical compartment.

2.4.3. Intestinal toxicity

Caco-2 cells were seeded at a density of 90,000 cells/cm^2 on flat bottom 96-well culture plates. Confluence was reached after 3-4 days in a CO_2 incubator at 37°C.

A. Water-soluble tetrazolium-1 (WST-1) viability assay

Caco-2 cells were incubated for 24 h at 37°C with 200 µL heterocycle solution (50 µM) in DMEM supplemented with 10 % FBS, 1 % nonessential amino acid, 100 IU/mL penicillin and 100 µg/mL streptomycin. The positive control consisted of 1 % SDS; blank medium was used as negative control. Subsequently, 20 µL of WST-1 cell proliferation reagent was added and the incubation was continued for 3 h. Absorbance was measured at 440 nm against a 630 nm reference with a TECAN Infinite M200 plate reader (Tecan Benelux, Mechelen, Belgium).

B. Lactate dehydrogenase (LDH) toxicity assay

Caco-2 cells were incubated for 24 h at 37°C with 200 µL heterocycle solution (50 µM) in HBSS supplemented with 25 mM glucose and 10 mM HEPES at pH 7.4. The positive control consisted of 1 % Triton-X 100; blank medium was used as negative control. Subsequently, 50 µL of Tris buffer (200 mM, pH 8), 50 µL sodium lactate (50 mM) and 50 µL of a mixture of phenazine methosulfate (0.9 mg/100 µL water), iodonitrotetrazolium chloride (3.3 mg/100 µL DMSO) and β-Nicotinamide adenine dinucleotide sodium salt from *Saccharomyces cerevisiae* (8.6 mg/2.3 mL water) were added to 50 µL of samples or control. After 10 min at room temperature absorbance was measured at 490 nm.

2.5. Classification of heterocycles in BCS and BDDCS

Heterocycles were categorized in the BCS and BDDCS based on their solubility, permeability and metabolism. Therefore, compounds were ranked according to these properties. Firstly, solubility was considered high (≥ 500 mg/250 mL), intermediate (10 mg/250 mL < x < 500 mg/250 mL) or poor (≤ 10 mg/250 mL). This type of non-binary classification approach was proposed recently (Macheras and Karalis, 2014). We propose these threshold values based on the highest doses of the 10 most prescribed drugs in the United States (www.imshealth.com). Secondly, high permeability was assumed at P_{app} values ≥ $10x10^{-6}$ cm/s in the Caco-2 model since the fraction absorbed in human associated with these permeability values was shown to be at least 90% based on data in our lab (Ingels et al., 2004).

For metabolism, ER was determined with the well-stirred model based on the $Cl_{H,met}$, as described in section 2.3.9. Subsequently, metabolism was considered high (ER > 0.7), intermediate (0.3 ≤ ER ≤ 0.7) or poor (< 0.3). In the BCS, heterocycles were categorized based on solubility and permeability: Class I (high solubility, high permeability), Class II (low solubility, high permeability), Class III (high solubility, low permeability) and Class IV (low solubility, low permeability). In the BDDCS, the compounds were classified based on solubility and metabolism: Class I (high solubility, extensive metabolism), Class II (low solubility, extensive metabolism), Class III (high solubility, poor metabolism) and Class IV (low solubility, poor metabolism) (Larregieu and Benet, 2014; Wu and Benet, 2005).

2.6. Glomerular filtration

Renal clearance through glomerular filtration ($Cl_{renal,filtration}$) was calculated as follows:

$$Cl_{renal,filtration} = f_u \text{ x GFR} \quad \text{(Equation 14)}$$

where GFR is the glomerular filtration rate in rats which was 1.31 mL/min in rats of 180 g (Davies and Morris, 1993).

2.7. HPLC analysis

The HPLC system used to analyze the heterocyclic compounds consisted of a Waters 2790 Alliance series separations module and a Novapak C18 column under radial compression (Waters, Milford, MA). UV absorbance was monitored using a Waters 2487 detector and fluorescence using a FP-1520 intelligent fluorescence detector (Jasco, Tokyo, Japan). The observed peaks were integrated using Empower Pro (Empower 2) software. The calibration curves of the heterocycles were linear over the concentration range of 0.78 µM to 100 µM. The different HPLC methods of heterocycles are listed in supplemental Table 1.

2.8. Statistics

Statistical analysis was performed using a two-tailed unpaired t-test. P-values of less than 0.05 are considered statistically significant.

In the hepatotoxicity assay, urea production in treated cells is expressed as fold change versus the untreated situation. Functionality and integrity of treated cells were considered significantly decreased when mean (+/- 95% C.I.) residual urea production fell below 67% of control values (test/reference ratio ≤ 2/3).

The Tanimoto coefficient was determined to evaluate similarity between compounds. This parameter is defined as *c/(a+b+c)*, which is the proportion of the features shared among two compounds divided by their union. The number of features (or on-bits in binary fingerprint) common in both compounds is indicated by *c*. The number of features unique in one or the other compound are indicated by *a* and *b*, respectively. The Tanimoto coefficient ranges between 0 and 1 with greater similarities indicated with higher values (Wuyts et al., 2013).

3. RESULTS

3.1. *In silico* profiling

Key physicochemical properties of the heterocycles are depicted in Table 1.

3.2. Hepatic disposition profiling

3.2.1. *In vitro* intrinsic uptake clearance in suspended rat hepatocytes

Hepatic uptake of all heterocycles at 37°C and 4°C in SRH is shown in Figure 2. For **1210**, **1211**, **1214**, **1269**, **1271**, **1348**, **1350**, **1396**, **1398** and **1399**, a significant difference was observed between 37°C and 4°C, indicating possible involvement of active uptake transporters. Therefore, these compounds were checked for hOATP1B-inhibition potential using a proteochemometrics-based *in silico* model (De Bruyn et al., 2013). However, none of the compounds was predicted to be a hOATP1B-inhibitor. To compare uptake rates from marker drugs from different BDDCS classes with the heterocycles, Figure 2 also includes marker drug from the four BDDCS classes (1) propranolol, (2) atorvastatin, (3) valsartan and (4) digoxin (Umehara and Camenisch, 2012). Only **1210** and **1367** exhibited uptake rates in the same range as these compounds; uptake of all other heterocycles was more pronounced.

3.2.2. *In vitro* intrinsic metabolic clearance in rats

$Cl_{int,met}$ of the heterocycles was determined in microsomes and hepatocytes. There was a poor correlation between $Cl_{int,met,hep}$ and $Cl_{int,met,mic}$, as illustrated in Figure 3. However, the generated data allow the classification of these compounds in different groups: (i) compounds only metabolized in hepatocytes, (ii) compounds more extensively metabolized in hepatocytes as compared to microsomes, (iii) compounds more extensively metabolized in microsomes as compared to hepatocytes and (iv) compounds that show a good correlation between $Cl_{int,met,hep}$ and $Cl_{int,met,mic}$. Metabolic clearance of **1210**, a chosen representative of the second group, was mainly mediated by cytochrome P450 (CYP) enzymes since 91% of metabolism was inhibited in the presence of ABT.

Therefore, a $Kp_{u,u}$ value of 4.77 could be calculated based on fu and Km values determined with microsomes and hepatocytes, shown in Table 2, indicating an accumulation of this compound in the intracellular compartment. **1269** was selected as a representative for the third group in which compounds are more extensively metabolized in microsomes compared to hepatocytes. Since efflux from hepatocytes could explain the inconsistency, canalicular and basolateral efflux were evaluated. However, no canalicular and limited basolateral clearance (0.44 ± 0.07 mL/min/kg bodyweight) of **1269** was observed.

3.2.3. Metabolic site prediction

MetaPrint2d was used to predict anilines, thiophenes and thiazoles to be most prone to metabolism for the heterocyclic compounds (Figure 4).

3.2.4. *In vitro – in vivo* extrapolation (IVIVE) of clearance in rats

To determine the rate-limiting step in the overall hepatic elimination of the heterocycles, *in vivo* hepatic clearance was predicted with the well-stirred model using $Cl_{int,uptake}$, $Cl_{int,met,hep}$ or a combination of both. With the exception of **1210**, total hepatic elimination of the heterocycles was poor or intermediate as indicated by the ER (Table 3). A weak correlation was observed between Cl_H and $Cl_{H,uptake}$ (R^2= 0.57; Figure 5A). On the contrary, a strong correlation was observed between Cl_H and $Cl_{H,met}$ (R^2= 0.96; Figure 5B), indicating that metabolism is the rate-limiting step in hepatic elimination of these heterocycles.

3.2.5. Hepatotoxicity

Hepatotoxicity data is shown in Figure 6. For 12 compounds after 6-72 h incubation periods, the urea production by hepatocytes was not significantly different from control. However, mean ratios of urea levels in cells treated with 50 µM of **1349**, **1350**, **1352** and **1365** were significantly decreased after 48 h. Except for wells incubated with **1365**, in which hepatocytes recovered, these cells showed hepatotoxicity after 72 h as well. Cells treated with **1213** started to show toxicity after 72 h of

408 treatment. Conversely, treatment of cells with 5 µM of compound did not influence the urea
409 production compared to the control situation for all heterocycles.

410 3.3. Intestinal disposition profiling

411 3.3.1. Intraluminal solubility

412 Figure 7 illustrates a broad range in solubility values of the heterocycles in FaSSIF, ranging from 0.40 ±
413 0.03 mg/250 mL for **1399** to 718 ± 133 mg/250 mL for **1210**.

414 3.3.2. Intestinal permeability

415 Similar as for the intraluminal solubility, a broad range was observed for permeability, as shown in
416 Figure 8 with P_{app} values ranging from 65.7 ± 5.6 x 10^{-6} cm/s for **1271** to 7.4 ± 1.4 x 10^{-6} cm/s for **1348**.
417 No significant increase in P_{app} values was observed in the presence of P-gp inhibitor GF120918
418 indicating that intestinal absorption is not influenced by P-gp. P_{app} values of all heterocycles were
419 higher than that of the paracellular marker atenolol (0.19 x 10^{-6} cm/s). Permeability for 6 heterocycles
420 was lower than that for the transcellular marker metoprolol (14.1 x 10^{-6} cm/s; **1211**, **1348**, **1349**, **1367**,
421 **1398**, and **1399**) whereas all other compounds exhibited higher P_{app} values (Figure 8).

422 3.3.3. Intestinal toxicity

423 No toxicity was observed with the WST-1 and LDH assay in Caco-2 cells treated with 50 µM of the
424 heterocycles for 24 h (data not shown).

425 3.4. Classification of heterocycles in BCS and BDDCS

426 Classification of the heterocycles in terms of their solubility, permeability and metabolism is shown in
427 Table 4. Since no biological activity has been determined for these compounds, solubility based on the
428 therapeutic dose was impossible to determine. Therefore, threshold values were selected to
429 determine high (≥ 500 mg/250 mL), intermediate (10 mg/250 mL < x < 500 mg/250 mL) or poor (≤ 10
430 mg/250 mL) solubility. According to BCS, **1210** exhibited high intestinal solubility and permeability and

could therefore be ranked as a Class I compound. **1271** and **1396** showed intermediate solubility and could either be categorized in Class I or II. All other compounds were Class II compounds, indicating low solubility and high permeability, although **1211**, **1348**, **1349** and **1399** could also be Class IV compounds since their permeability was only intermediate.

Since most compounds exhibited both poor solubility and poor metabolism, almost all heterocycles were classified as Class IV compounds in BDDCS. However, due to its extensive metabolism and high solubility, **1210** was considered as a Class I compound. Intermediate metabolism was observed for **1214** and **1270**; hence these compounds could be classified under Class II or IV. Conversely, **1271** showed intermediate solubility and could therefore be either Class III or IV. Finally, both solubility and metabolism were intermediate for **1396;** consequently this heterocycle can belong to all four classes.

4. DISCUSSION

The aim of this study was to apply pre-clinical models to predict ADMET properties of 19 heterocycles with structures that frequently occur in drugs and lead compounds (e.g. duloxetine, clopidogrel) (Gomtsyan, 2012).Adequate *in vitro* models were used to determine the compounds' intestinal solubility and permeability and hepatic metabolism to classify the compounds according to BCS and BDDCS and predict oral absorption and hepatic elimination.

In silico determination of physicochemical properties predicted all compounds to be conform with Lipinski's rule of five (Lipinski et al., 2001) (Table 1), indicating that based on (i) the amount of HB_a and HB_d; (ii) MW , and (iii) LogD poor intestinal absorption and permeation are unlikely (Lipinski et al., 2001). In addition, the low number of rotatable bonds (<10) and PSA-values of 140 $Å^2$ or less indicated good oral bioavailability (Veber et al., 2002). However, despite favorable physicochemical properties, extensive biopharmaceutical profiling was considered necessary to accurately predict ADMET properties.

First, hepatic disposition was evaluated. Hepatic uptake, measured in suspended hepatocytes, was mainly passive (Figure 2) for these relatively small compounds which are neutral at physiological pH, since uptake was relatively high at 4˚C. However, uptake of ten compounds was significantly decreased at this low temperature indicating that active transport might be involved. It should be noted that a major limitation of this method is the altered membrane fluidity at 4°C which could limit the uptake (Zamek-Gliszczynski et al., 2013). Although transporters involved in heterocycle uptake have not been identified, the compounds were evaluated in a proteochemometrics-based *in silico* model to check for hOATP-inhibition potential. None of the compounds was expected to inhibit isoform 1B1 or 1B3 of this transporter which are mainly susceptible to anionic compounds (De Bruyn et al., 2013).

Hepatic metabolic stability was investigated in RLM and SRH. As shown in Figure 3, a poor correlation was observed between the different *in vitro* systems. However, the plot allowed a classification of the heterocycles in groups: (i) compounds which were only metabolized in hepatocytes; (ii) compounds

more extensively metabolized in hepatocytes compared to microsomes; (iii) compounds more extensively metabolized in microsomes compared to hepatocytes and (iv) compounds that showed a good correlation between $Cl_{int,met,hep}$ and $Cl_{int,met,mic}$. Although microsomes have been the principal model to study metabolic clearance, they show some disadvantages which could explain the inconsistency depicted in Figure 3. First of all, microsomes do not contain cytosolic enzymes, in particular most phase II enzymes (e.g. N-acetyltransferases or sulfotransferases). Moreover, uridine 5'-diphospho-glucuronosyltransferases are only active in the presence of their co-factor. This might result in the limited microsomal metabolism of compounds from the first and second group (Obach, 1999; Parker and Houston, 2008). For these compounds, hepatocytes containing all hepatic enzymes should be considered to evaluate metabolic stability in addition to microsomes. However, despite their biorelevance and the increasing importance of phase II enzymes in the elimination of NCE's, a major drawback of using hepatocytes is the availability and cost of human hepatocytes. Despite the presence of multiple sites potentially susceptible to metabolism (Figure 4), compounds **1348**, **1349** and **1399** are not metabolized in microsomes and only poorly in hepatocytes (Figure 3). Consequently, alternative methods should be considered to evaluate the turnover of those slowly metabolized compounds. The relay method, using several batches of thawed hepatocytes could be applied. Alternatively, hepatocyte culture systems with sustained drug-metabolizing activities might be used (Di and Obach, 2015). In addition to the absence of certain enzymes, microsomes lack cellular context and therefore ignore the possible role of membrane transporters (Ito and Houston, 2004; Parker and Houston, 2008; Webborn et al., 2007). Hence, concentrations at the enzyme level in microsomes are equal to the applied concentrations during the incubation. On the contrary, in hepatocytes, accumulation of compound at the enzyme site could occur which possibly enhances the apparent intrinsic clearance in this model system (Chu et al., 2013). Indeed, table 1 predicted hepatic accumulation of all heterocycles studied here ($K_{liver:blood} > 1$). Interestingly, accumulation of unbound **1210**, a representative from group 2 in Figure 3, occurred. This heterocycle showed a $Kp_{u,u}$ value of 4.77, which explains the increased metabolism of this compound in hepatocytes since unbound compound, which is considered to be the

493 relevant fraction of compound interacting with metabolizing enzymes, is reaching almost 5-fold higher
494 concentrations inside hepatocytes. On the contrary, a lower concentration at the enzyme level in
495 hepatocytes compared to microsomes was proposed for group 3 in Figure 3. These lower
496 concentrations could occur when efflux predominates; however efflux was only limited for compound
497 **1269**. Alternatively, extensive intracellular binding or sequestration in organelles could also limit
498 compound availability for enzymes. Therefore, accurate knowledge regarding intracellular drug
499 exposure in addition to systemic (plasma) exposure is crucial to gain mechanistic understanding of
500 drug exposure to metabolizing enzymes (Nicolaï et al., 2015).

501 Metaprint2d predicted a high likelihood of metabolism on anilines, thiophenes and thiazoles (Figure
502 4). The aniline moiety was present in both **1210** and **1396**. Since no degradation of **1396** was observed
503 in microsomes, non-microsomal metabolism (e.g. phase II) is most likely for this compound. Possible
504 phase II reactions on anilines are acylation, glucuronidation and formylation. Interestingly, although
505 phase I metabolism was predicted for all compounds in the first group, no metabolism could be
506 observed in microsomes. However, it should be noted that the findings of this prediction model are
507 restricted to the number and diversity of compounds used in the database to construct the model
508 (http://www-metaprint2d.ch.cam.ac.uk/).

509 IVIVE has successfully been applied for compounds of which elimination is predominantly mediated by
510 uptake transporters or metabolic enzymes (Ito and Houston, 2004; Watanabe et al., 2010). However,
511 the clearance of most compounds results from a complex interplay between both processes.
512 Therefore, models have been developed implementing multiple processes of hepatic elimination
513 (Umehara and Camenisch, 2012; Webborn et al., 2007). To evaluate the rate-limiting step in the overall
514 hepatic elimination, the *in vivo* clearance of the heterocycles was predicted with the well-stirred-
515 model based on uptake, metabolism or a combination of both. Hepatic clearance based on uptake data
516 resulted in a poor correlation (R^2=0.57) with hepatic clearance based on the combination of both
517 processes. Hepatic clearance based on uptake over-predicted the total hepatic clearance (Figure 5A).

Conversely, *in vivo* hepatic clearance based on metabolism resulted in a strong correlation (R^2=0.96) with the hepatic clearance based on a combination of uptake and metabolism, suggesting that hepatic metabolism was more important in the hepatic elimination (Figure 5B). Consequently, drug-drug-interactions at the enzyme-level may be anticipated for these heterocycles. Subsequently, ER were calculated based on total hepatic *in vivo* clearance predictions. Poorly cleared compounds are favorable when side effects are not an issue and when prolonged contact with the target is necessary for the treatment. Extensively cleared compounds could be useful when inactive prodrugs need to be converted into active metabolites. Compound **1210** is the only compound for which extensive clearance was predicted. Metabolism of this compound in hepatocytes was relatively high as indicated in Figure 3. Moreover, plasma protein binding of **1210** (69%) was relatively low as compared to the other compounds (86-99%). Since biological activity of the heterocycles still needs to be evaluated, compounds with poor or intermediate ER are most promising for once daily dosing regimens.

Hepatotoxicity of the heterocycles was determined in SCRH with a urea assay, evaluating biochemical integrity and functionality of hepatocytes (Chatterjee et al., 2014). For **1349**, **1350** and **1352** toxicity was observed when cells were incubated for 48 and 72 h with 50 µM of the compound, indicated by a significant decrease (> 33 %) in urea production. The urea production in cultures treated with **1213** decreased over time as well. However, this reduction was only significant after 72 h. Interestingly, toxicity for **1365** was observed after 48 h, but not after 72 h meaning the cells recovered after the second urea assay. This recovery can imply that the observed toxicity resulted from exposure to a phase I metabolite which is subsequently eliminated by phase II metabolism. None of the compounds were considered toxic after incubations with 5 µM.

Intestinal solubility and permeability were determined to evaluate pre-systemic disposition using FaSSIF, containing mixed micelles of taurocholate and lecithin. We previously demonstrated a strong correlation between solubility in FaSSIF and fasted state human intestinal fluid for 17 model compounds (Clarysse et al., 2011). Notwithstanding similar physicochemical properties, the different

543 substitutions had a major effect on the solubility of the heterocycles, demonstrated by a broad range
544 in solubility values, ranging from 0.40 ± 0.03 mg/250 mL to 718 ± 133 mg/250 mL. For example, a furan
545 moiety on **1352** resulted in an 11-fold higher solubility compared to the more lipophilic thiophene
546 group in **1348** (Tanimoto coefficient 0.85). A similar difference between **1271** and **1211** changed the
547 solubility 2.3-fold (Tanimoto coefficient 0.81). On the contrary, the effect on solubility of an altered
548 bicyclic moiety on structurally similar molecules was less pronounced (e.g**. 1269** and **1349** or **1350** and
549 **1365**). Moreover, prolongation of the aliphatic chain in **1269** and **1270** compared to **1211** and **1214**
550 resulted in a 4- and 7-fold increase in solubility, respectively. These pairs of compounds exhibit the
551 same physicochemical properties, as illustrated in Table 1, except for the number of RB. The extra RB
552 resulted in more flexible molecules that could adapt their conformation to the polarity of the
553 environment (e.g. FaSSIF medium) which can explain the increase in solubility (Navia and Chaturvedi,
554 1996). As indicated in Figure 7, most heterocycles are classified as poorly soluble compounds and
555 hence predisposed to low oral bioavailability. However, highly soluble compounds are preferred to be
556 enrolled in the drug development process. Nevertheless, the improved understanding of approaches
557 that promote solubility in the gastrointestinal tract has allowed the successful introduction of many
558 drugs that are considered poorly soluble on the market (Williams et al., 2013) The approaches include
559 particle size reduction, modification of the crystal habit, complexation, drug dispersion in carriers, the
560 addition of surfactans or chemical modifications (Singh et al., 2011; Williams et al., 2013).Intestinal
561 permeability was also highly affected by the substitutions present in the heterocyclic structures,
562 resulting in a broad range of P_{app} values. Permeability of all heterocycles was higher than that of the
563 paracellular marker atenolol ($0.19x10^{-6}$ cm/s). For 6 heterocycles P_{app} was lower than that of the
564 transcellular marker metoprolol (Figure 8: **1211**, **1348, 1349**, **1367**, **1398** and **1399**) whereas all other
565 compounds showed higher P_{app} values (Figure 8). Based on previous data from our lab, compounds
566 with P_{app} values of $10x10^{-6}$ cm/s and higher are considered to exhibit a fraction absorbed in human of
567 at least 90% (Ingels et al., 2004). Therefore, 13 heterocycles were expected to be well absorbed (Figure
568 8). Moreover, the intestinal absorption of none of the compounds will be limited by the efflux

transporter P-gp since their permeability was unaffected in the presence of P-gp-inhibitor GF120918 (elacridar). In general, high permeability is observed for more lipophilic compounds. However, the P_{app} values determined for **1211** and **1348** were markedly lower than for **1271** and **1352** although the latter were more hydrophilic. A possible explanation may be that the lipophilic **1211** and **1348** reside in the micelles of the medium, lowering the free fraction of compound available for permeation across the Caco-2 monolayer.

Heterocycles were categorized according to BCS and BDDCS which are useful tools in early stages of drug discovery (Table 4). These classifications predict absorption and routes of drug elimination respectively. Originally a compound was defined as 'highly soluble' when the highest dose strength on the market is soluble in 250 mL or less of aqueous medium (Wu and Benet, 2005). However, since no biological activity for these heterocycles has been determined yet, we propose threshold values based on the highest doses of 10 most prescribed drugs in the United States (www.imshealth.com). All categories contained compounds from this list: (i) highly soluble compounds (≥500 mg/250 mL): acetaminophen, metformin, azithromycin; (ii) intermediately soluble compounds (10 mg/250 mL < x < 500 mg/250 mL): simvastatin, lisinopril, omeprazole; and (iii) poorly soluble compounds (≤10 mg/250 mL): hydrocodone, levothyroxine, amlodipine and alprazolam. Moreover, the ranking allowed application of BCS and BDDCS for NCE's, prior to *in vivo* administration in humans. Importantly, when dosages of these compounds appear to be relatively low, heterocycles may have to be considered highly soluble instead of poorly or intermediately soluble. With respect to permeability, metoprolol has previously been chosen as a high permeability reference cut-off for 90% absorption of the oral dose (Larregieu and Benet, 2014). However, since metoprolol possibly resides in micelles of the FaSSIF medium used in this study we used a cut-off P_{app} value of $10x10^{-6}$ cm/s or higher in Caco-2 cells as described earlier (Ingels et al., 2004). An ER of >70% calculated with the $Cl_{int,met,hep}$ in the well-stirred model indicated extensive metabolism (Wuyts et al., 2013).

593 It has been suggested that BCS Class I and II compounds are extensively metabolized. Indeed,
594 metabolism of **1210** will not be limited by solubility or permeability and is considered a Class I
595 compound in both BCS and BDDCS. Nevertheless, regardless of high permeability, most heterocyclic
596 compounds were poorly metabolized. Therefore, most heterocycles were class IV compounds in the
597 BDDCS whereas the BCS mainly resulted in class II compounds.

598 Class IV compounds are expected to be excreted unchanged. However, no canalicular excretion has
599 been detected for compound **1269** and the molecular weight of the compounds were below the cut-
600 off value above which biliary excretion is expected (Yang et al., 2010). Moreover, renal clearance
601 through glomerular filtration was relatively low compared to hepatic clearance (Supplemental Table
602 2). Nevertheless, active processes in the kidney could still be involved. Furthermore, poor metabolism
603 for compounds with a high permeability rate as well as high hepatic uptake might be explained by
604 extensive intracellular binding or organelle sequestration. Moreover, the inconsistency between the
605 BCS and BDDCS could result from the binary structure of these systems. For compound classification,
606 the criteria solubility, permeability and metabolism are evaluated as either high/low or
607 poor/extensive. However, a continuity for these properties has been observed in the current study
608 (Figure 3, 7 and 8) as well as in previous research (Macheras and Karalis, 2014). Therefore, the
609 classification of a large number of compounds in the BCS and BDDCS, specifically compounds with
610 moderate solubility, permeability or metabolism, is uncertain. Consequently, systems with a
611 continuous nature have been developed which are complementary to the conventional binary
612 systems. For example, Macheras and Karalis introduced the ABΓ system that allowed the prediction of
613 the fraction of the dose absorbed (Fa) in a quantitative manner for compounds with low, moderate
614 and high solubility or permeability in classes A ($Fa \geq 0.90$), Γ ($0.20 \geq Fa \geq 0.90$) and B ($Fa \leq 0.20$).
615 Notwithstanding the authors compared the ABΓ system to the BCS, their findings can also be related
616 to the BDDCS as permeability in the BCS was replaced by metabolism in the BDDCS (Macheras and
617 Karalis, 2014). The non-binary character of the ABΓ system provides extra information regarding the
618 fraction absorbed which more accurately predicts this parameter for compounds with moderate

619 solubility, permeability and metabolism in particular. In addition, the ABΓ system facilitates the
620 understanding of the discrepancy between BCS and BDDCS. Finally, it should be noted that the *in vitro*
621 models used for the classification originate from different species. The Caco-2 cells used to determine
622 intestinal permeability is a human cell line derived from colonic adenocarcinoma while metabolism
623 studies have been performed in rat hepatocytes. Species-specific differences can be expected although
624 poor metabolism in rat probably indicates poor metabolism in human since rodents tend to eliminate
625 drugs faster than humans (Martignoni et al., 2006).

626 ## 5. CONCLUSION

627 In addition to microsomes, hepatocytes should be included as a standard *in vitro* model system to
628 cover potential involvement of phase II enzymes and cellular accumulation of unbound compound due
629 to transporter-mediated processes. Therefore, accurate knowledge regarding intracellular drug
630 exposure should be obtained with methods that allow measurements of the unbound drug
631 concentrations in intact hepatocytes. Additionally, the *in vitro* data regarding solubility, permeability
632 and metabolism was used for the the classification of NCE's in the BCS and BDDCS to predict drug
633 disposition characteristics before clinical data is available.

634 Most heterocycles evaluated in this study show reasonable drug-like properties. At the level of the
635 intestine, 13 compounds demonstrated high permeability (>10x10^{-6} cm/s) and no toxicity. The limited
636 solubility could be overcome by proper formulation strategies. At the hepatic level, compounds were
637 taken up easily and metabolism, which was intermediate or poor (except for **1210**), was the rate-
638 limiting step in the elimination. Hepatotoxicity was limited at 50 µM and absent at 5 µM. The
639 compounds were mainly classified as class II compounds in BCS and class IV compounds in BDDCS.

6. LEGENDS

Figure 1: Chemical structures of the heterocycles investigated in the present study.

Figure 2: Accumulation of heterocycles in suspended rat hepatocytes following uptake (1 min; 8 µM) at 37°C (black bars) and 4°C (white bars) is presented as the mean + S.D. (n=3). Marker drugs from different BDDCS classes are shown: (1) propranolol, (2) atorvastatin, (3) valsartan and (4) digoxin (Umehara and Camenisch, 2012).

Figure 3: Scaled intrinsic clearance of the heterocycles determined in rat hepatocytes versus rat liver microsomes (8 µM). The solid line represents identical values in both model systems. Group I – IV are indicated in boxes.

Figure 4: Prediction of most likely metabolized sites of the heterocycles using Metaprint2d. Normalized occurrence ratios (NOR) were indicated: 1:0.66 ≤ NOR ≤ 1; 2:0.33 ≤ NOR ≤ 0.66 and; 3:0.15 ≤ NOR ≤ 0.33. Group I – IV are indicated.

Figure 5: Relationship between intrinsic *in vivo* clearance values based on uptake data only ($Cl_{H,uptake}$) versus the combination of uptake and metabolism (Cl_H) (A) or metabolism data only ($Cl_{H,met}$) versus Cl_H (B).The solid line represents the regression curve and the dashed lines the plasma flow in rats.

Figure 6: The mean ratio of urea production in treated vs. control cells + 95% C.I. (n=3). A urea assay was performed after incubation with 50 µM of the heterocycles for 6 (black bars), 48 (grey bars) and 72 (white bars) h.

Figure 7: Solubility of the heterocycles (mg/250 mL) and metoprolol in FaSSIF is presented as the mean + S.D. (n=3). Solubility was considered high (≥ 500 mg/250 mL), intermediate (10 mg/250 mL < x < 500 mg/250 mL) or poor (≤ 10 mg/250 mL).

Figure 8: Absorption potential of the heterocycles and marker drugs in FaSSIF using the Caco-2 model in absence (black bars) and presence (white bars) of 4µM P-glycoprotein inhibitor GF-120918

663 (elacridar) is presented as the mean + S.D. (n=3). Marker drugs include a transcellular marker
664 (metoprolol), a paracellular marker (atenolol) and a P-gp substrate (indinavir).

665

666

7. REFERENCES

Annaert, P.P., Turncliff, R.Z., Booth, C.L., Thakker, D.R., Brouwer, K.L., 2001. P-glycoprotein-mediated in vitro biliary excretion in sandwich-cultured rat hepatocytes. Drug Metab. Dispos. 29, 1277–83.

Chatterjee, S., Richert, L., Augustijns, P., Annaert, P., 2014. Hepatocyte-based in vitro model for assessment of drug-induced cholestasis. Toxicol. Appl. Pharmacol. 274, 124–36.

Chiba, M., Hensleigh, M., Lin, J.H., 1997. Hepatic and intestinal metabolism of indinavir, an HIV protease inhibitor, in rat and human microsomes. Major role of CYP3A. Biochem. Pharmacol. 53, 1187–95.

Chiba, M., Ishii, Y., Sugiyama, Y., 2009. Prediction of hepatic clearance in human from in vitro data for successful drug development. AAPS J. 11, 262–76.

Chu, X., Korzekwa, K., Elsby, R., Fenner, K., Galetin, A., Lai, Y., Matsson, P., Moss, A., Nagar, S., Rosania, G.R., Bai, J.P.F., Polli, J.W., Sugiyama, Y., Brouwer, K.L.R., 2013. Intracellular drug concentrations and transporters: measurement, modeling, and implications for the liver. Clin. Pharmacol. Ther. 94, 126–41.

Clarysse, S., Brouwers, J., Tack, J., Annaert, P., Augustijns, P., 2011. Intestinal drug solubility estimation based on simulated intestinal fluids: comparison with solubility in human intestinal fluids. Eur. J. Pharm. Sci. 43, 260–9.

De Bruyn, T., Fattah, S., Stieger, B., Augustijns, P., Annaert, P., 2011. Sodium fluorescein is a probe substrate for hepatic drug transport mediated by OATP1B1 and OATP1B3. J. Pharm. Sci. 100, 5018–30.

De Bruyn, T., van Westen, G., Ijzerman, A., Stieger, B., de Witte, P., Augustijns, P., Annaert, P., 2013. Structure-based identification of OATP1B1/3 inhibitors. Mol. Pharmacol. 83, 1257–67.

Di, L., Feng, B., Goosen, T.C., Lai, Y., Steyn, S.J., Varma, M. V, Obach, R.S., 2013. A perspective on the prediction of drug pharmacokinetics and disposition in drug research and development. Drug Metab. Dispos. 41, 1975–93.

Di, L., Obach, R.S., 2015. Addressing the Challenges of Low Clearance in Drug Research. AAPS J. 17, 352–357.

Fan, J., de Lannoy, I., 2014. Pharmacokinetics. Biochem. Pharmacol. 87, 93–120.

Gomtsyan, A., 2012. Heterocycles in drugs and drug discovery. Chem. Heterocycl. Compd. 48, 7–10.

http://www-metaprint2d.ch.cam.ac.uk/ [WWW Document], n.d. URL http://www-metaprint2d.ch.cam.ac.uk/ Last accessed 01/12/2014

Ingels, F., Beck, B., Oth, M., Augustijns, P., 2004. Effect of simulated intestinal fluid on drug permeability estimation across Caco-2 monolayers. Int. J. Pharm. 274, 221–32.

701 Ito, K., Houston, J.B., 2004. Comparison of the use of liver models for predicting drug clearance using
702 in vitro kinetic data from hepatic microsomes and isolated hepatocytes. Pharm. Res. 21, 785–
703 92.

704 Jang, M.-Y., Lin, Y., De Jonghe, S., Gao, L.-J., Vanderhoydonck, B., Froeyen, M., Rozenski, J., Herman,
705 J., Louat, T., Van Belle, K., Waer, M., Herdewijn, P., 2011. Discovery of 7-N-
706 piperazinylthiazolo[5,4-d]pyrimidine analogues as a novel class of immunosuppressive agents
707 with in vivo biological activity. J. Med. Chem. 54, 655–68.

708 Larregieu, C.A., Benet, L.Z., 2014a. Distinguishing between the permeability relationships with
709 absorption and metabolism to improve BCS and BDDCS predictions in early drug discovery. Mol.
710 Pharm. 11, 1335–44.

711 Larregieu, C.A., Benet, L.Z., 2014b. Distinguishing between the permeability relationships with
712 absorption and metabolism to improve BCS and BDDCS predictions in early drug discovery. Mol.
713 Pharm. 11, 1335–44.

714 Lipinski, C. a, Lombardo, F., Dominy, B.W., Feeney, P.J., 2001. Experimental and computational
715 approaches to estimate solubility and permeability in drug discovery and development settings.
716 Adv. Drug Deliv. Rev. 46, 3–26.

717 Macheras, P., Karalis, V., 2014. A non-binary biopharmaceutical classification of drugs: the ABΓ
718 system. Int. J. Pharm. 464, 85–90.

719 Martignoni, M., Groothuis, G.M.M., de Kanter, R., 2006. Species differences between mouse, rat,
720 dog, monkey and human CYP-mediated drug metabolism, inhibition and induction. Expert Opin.
721 Drug Metab. Toxicol. 2, 875–94.

722 Nakakariya, M., Ono, M., Amano, N., Moriwaki, T., Maeda, K., Sugiyama, Y., 2012. In vivo biliary
723 clearance should be predicted by intrinsic biliary clearance in sandwich-cultured hepatocytes.
724 Drug Metab. Dispos. 40, 602–9.

725 Navia, M.A., Chaturvedi, P.R., 1996. Design principles for orally bioavailable drugs. Drug Discov.
726 Today 6446, 179–189.

727 Nicolaï, J., De Bruyn, T., Van Veldhoven, P.P., Keemink, J., Augustijns, P., Annaert, P., 2015. Verapamil
728 hepatic clearance in four preclinical rat models: towards activity-based scaling. Biopharm. Drug
729 Dispos.

730 Obach, R.S., 1999. Prediction of human clearance of twenty-nine drugs from hepatic microsomal
731 intrinsic clearance data: An examination of in vitro half-life approach and nonspecific binding to
732 microsomes. Drug Metab. Dispos. 27, 1350–9.

733 Paixão, P., Aniceto, N., Gouveia, L.F., Morais, J.A.G., 2014. Prediction of Drug Distribution in Rat and
734 Humans Using an Artificial Neural Networks Ensemble and a PBPK Model. Pharm. Res. 31,
735 3313–22.

736 Parker, A.J., Houston, J.B., 2008. Rate-limiting steps in hepatic drug clearance: comparison of
737 hepatocellular uptake and metabolism with microsomal metabolism of saquinavir, nelfinavir,
738 and ritonavir. Drug Metab. Dispos. 36, 1375–84.

739 Singh, A., Worku, Z.A., Van den Mooter, G., 2011. Oral formulation strategies to improve solubility of
740 poorly water-soluble drugs. Expert Opin. Drug Deliv. 5, 367-83

741 Umehara, K.I., Camenisch, G., 2012. Novel in vitro-in vivo extrapolation (IVIVE) method to predict
742 hepatic organ clearance in rat. Pharm. Res. 29, 603–17.

743 Veber, D.F., Johnson, S.R., Cheng, H.-Y., Smith, B.R., Ward, K.W., Kopple, K.D., 2002. Molecular
744 properties that influence the oral bioavailability of drug candidates. J. Med. Chem. 45, 2615–23.

745 Wang, J., Urban, L., 2004. The impact of early ADME profiling on drug discovery and development
746 strategy. Drug Discov. world Fall, 73–86.

747 Watanabe, T., Kusuhara, H., Maeda, K., Kanamaru, H., Saito, Y., Hu, Z., Sugiyama, Y., 2010.
748 Investigation of the rate-determining process in the hepatic elimination of HMG-CoA reductase
749 inhibitors in rats and humans. Drug Metab. Dispos. 38, 215–22.

750 Webborn, P.J.H., Parker, a. J., Denton, R.L., Riley, R.J., 2007. In vitro-in vivo extrapolation of hepatic
751 clearance involving active uptake: theoretical and experimental aspects. Xenobiotica. 37, 1090–
752 109.

753 Williams, H.D., Trevaskis, N.L., Charman, S. a, Shanker, R.M., Charman, W.N., Pouton, C.W., Porter,
754 C.J.H., 2013. Strategies to address low drug solubility in discovery and development. Pharmacol.
755 Rev. 65, 315–499.

756 Wu, C.-Y., Benet, L.Z., 2005a. Predicting Drug Disposition via Application of BCS:
757 Transport/Absorption/ Elimination Interplay and Development of a Biopharmaceutics Drug
758 Disposition Classification System. Pharm. Res. 22, 11–23.

759 Wu, C.-Y., Benet, L.Z., 2005b. Predicting Drug Disposition via Application of BCS:
760 Transport/Absorption/ Elimination Interplay and Development of a Biopharmaceutics Drug
761 Disposition Classification System. Pharm. Res. 22, 11–23.

762 Wuyts, B., Keemink, J., De Jonghe, S., Annaert, P., Augustijns, P., 2013. Biopharmaceutical profiling of
763 a pyrido[4,3-d] pyrimidine compound library. Int. J. Pharm. 455, 19–30.

764 www.imshealth.com Last accessed 01/12/2014

765 Yang, X., Gandhi, Y. a, Morris, M.E., 2010. Biliary excretion in dogs: evidence for a molecular weight
766 threshold. Eur. J. Pharm. Sci. 40, 33–7.

767 Zamek-Gliszczynski, M.J., Lee, C. a, Poirier, A., Bentz, J., Chu, X., Ellens, H., Ishikawa, T., Jamei, M.,
768 Kalvass, J.C., Nagar, S., Pang, K.S., Korzekwa, K., Swaan, P.W., Taub, M.E., Zhao, P., Galetin, A.,
769 2013. ITC recommendations for transporter kinetic parameter estimation and translational
770 modeling of transport-mediated PK and DDIs in humans. Clin. Pharmacol. Ther. 94, 64–79.

771

8. ACKNOWLEDGEMENTS

Financial support for this research was provided by the Institute for the promotion of Innovation by Science and Technology in Flanders (IWT) under Grant SBO-IWT.

Figure 1

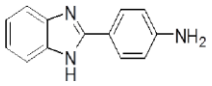

1210

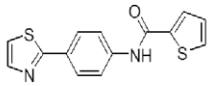

1211

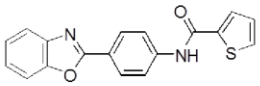

1213

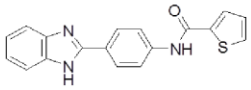

1214

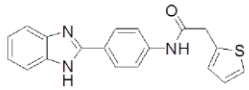

1269

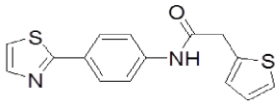

1270

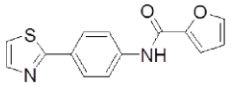

1271

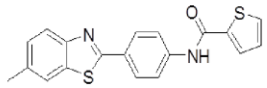

1348

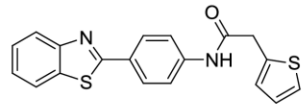

1349

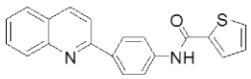

1350

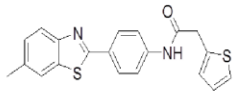

1351

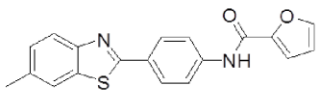

1352

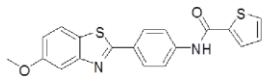

1354

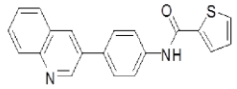

1365

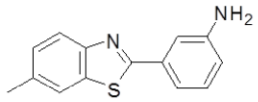

1366

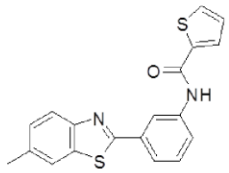

1367

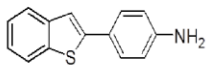

1396

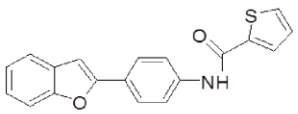

1398

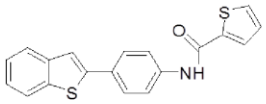

1399

776

777

Figure 2

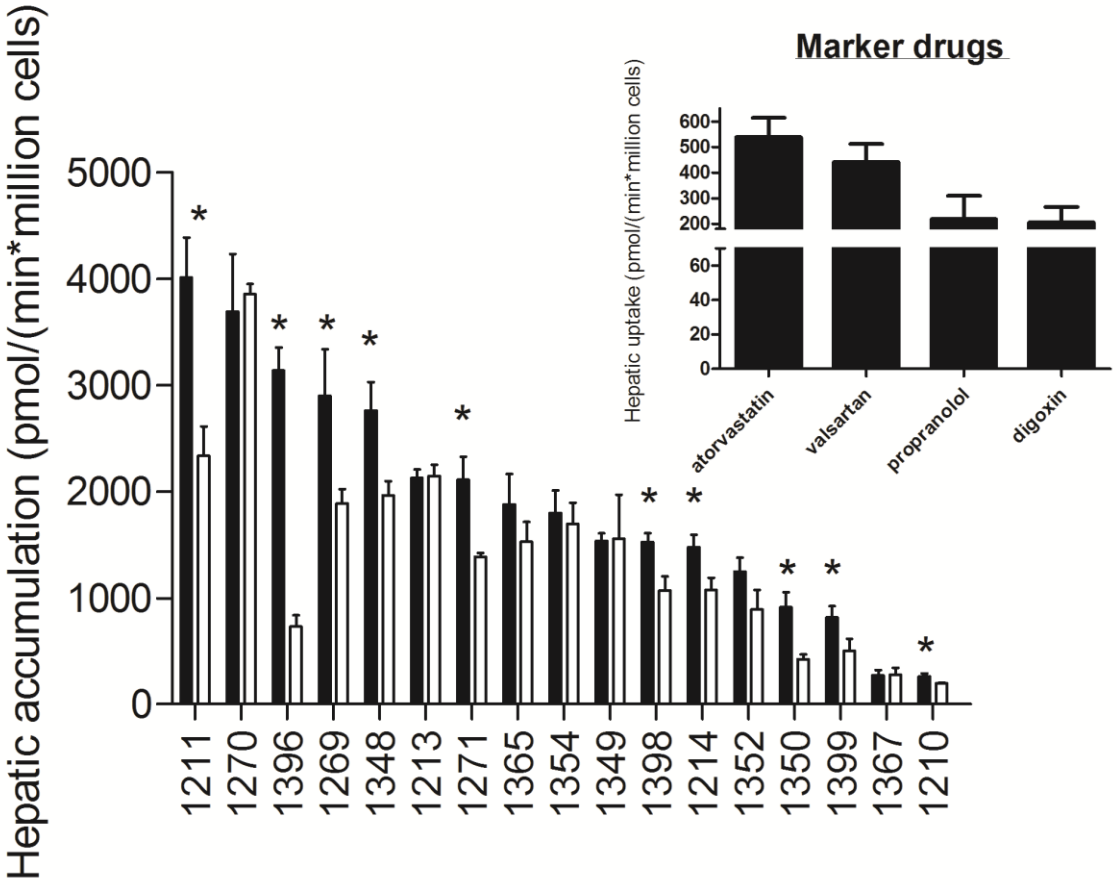

778

779

Figure 3

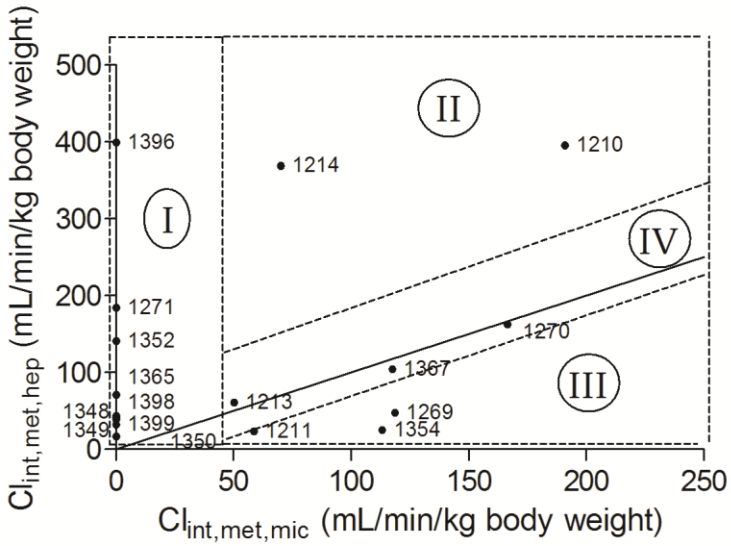

780

781

Figure 4

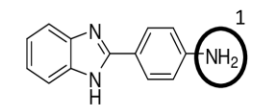

1210 (II)

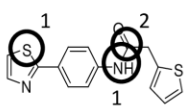

1270 (IV)

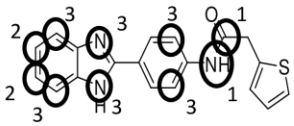

1269 (III)

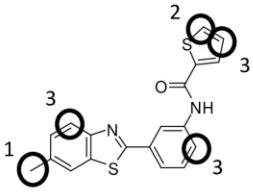

1367 (IV)

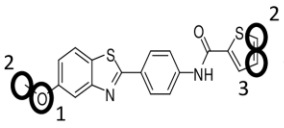

1354 (III)

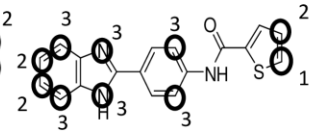

1214 (II)

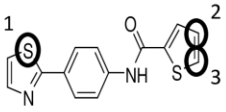

1211 (III)

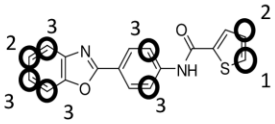

1213 (IV)

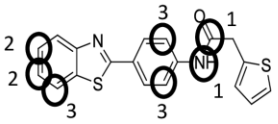

1349 (I)

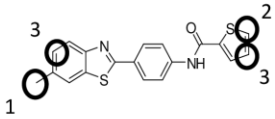

1348 (I)

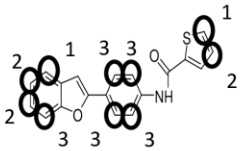

1398 (I)

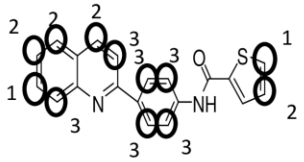

1350 (I)

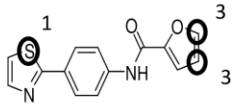

1271 (I)

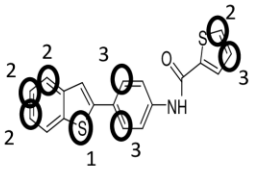

1399 (I)

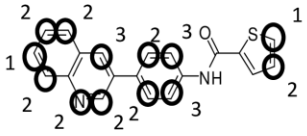

1365 (H)

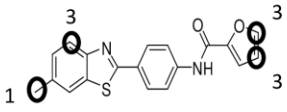

1352 (H)

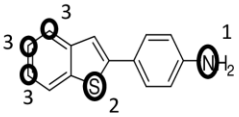

1396 (H)

782

783

A.

Figure 5

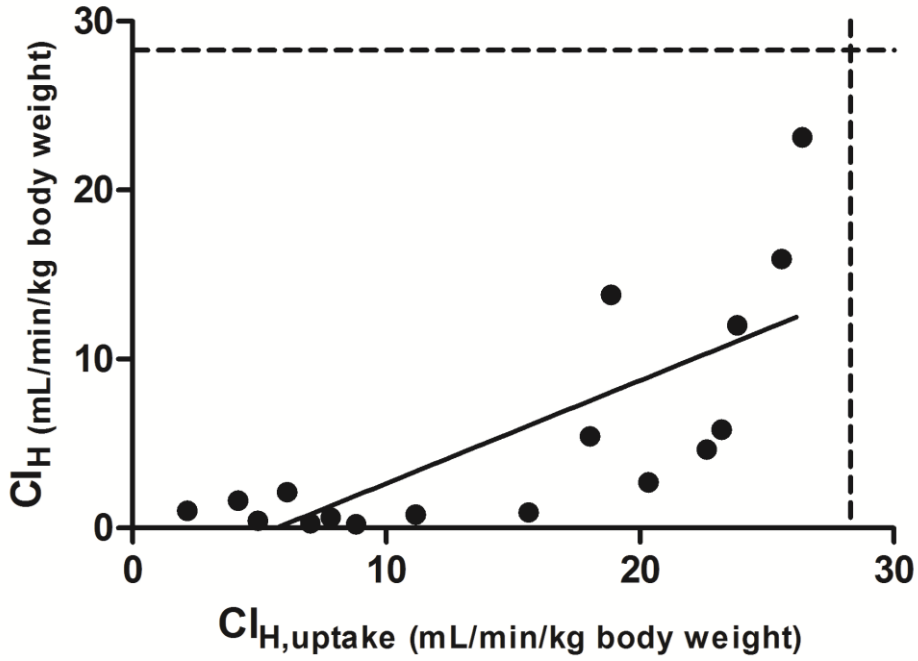

B.

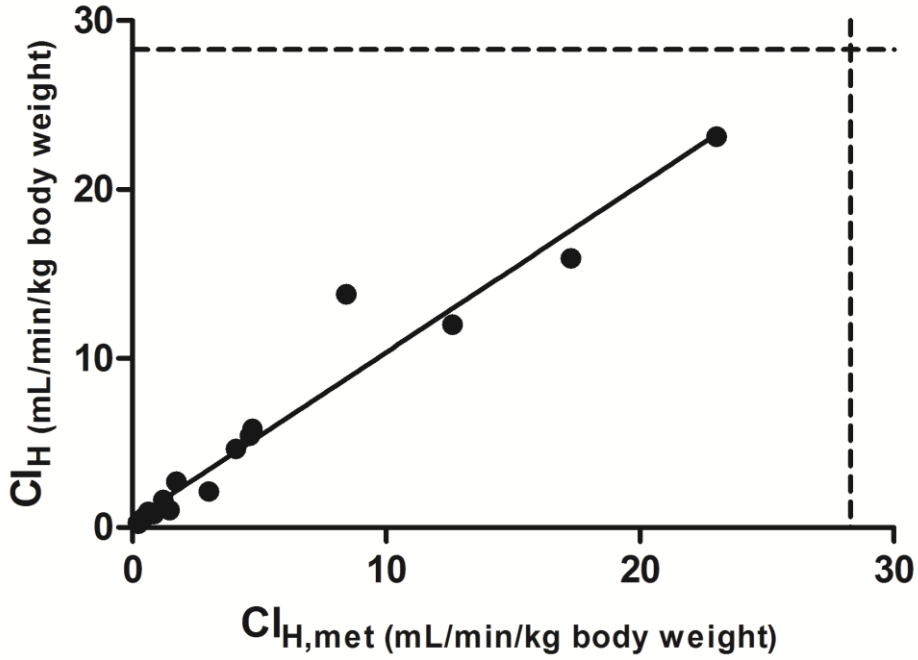

784

785

Figure 6

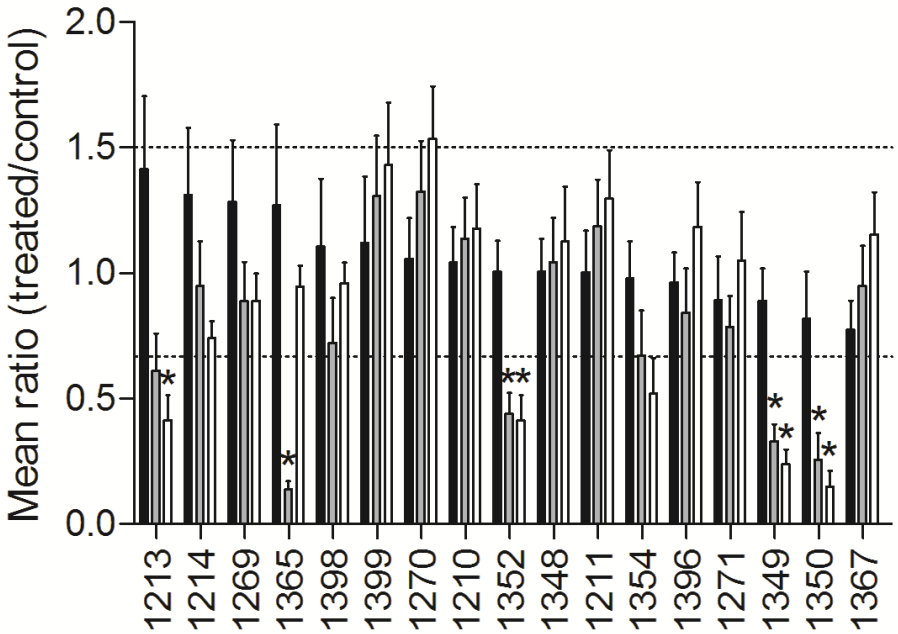

786

787

Figure 7

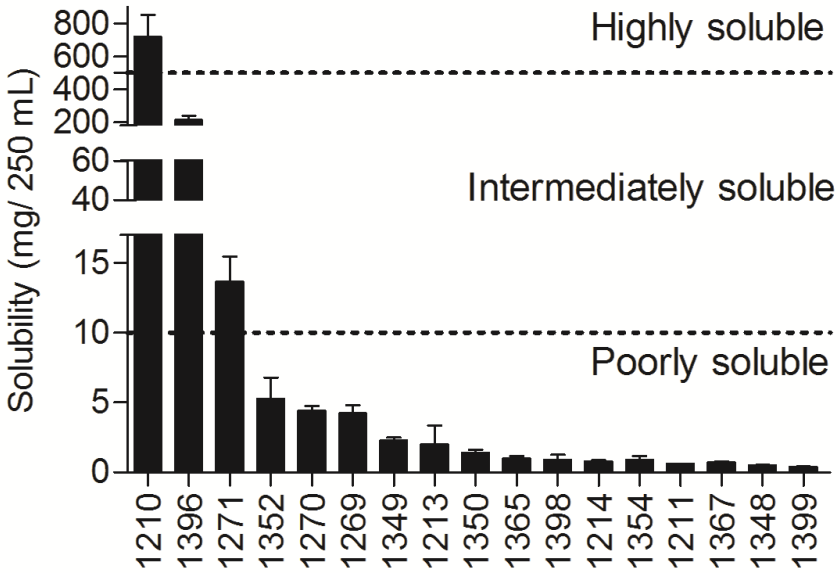

788

789

Figure 8

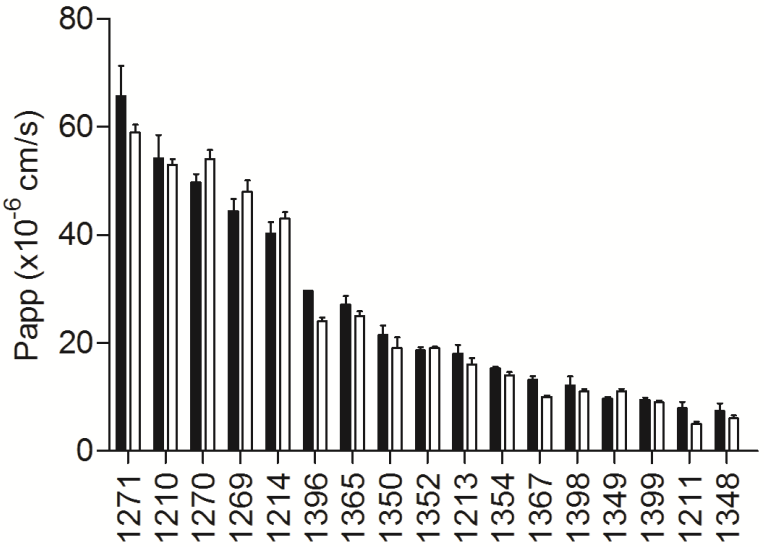

790

791

Table 1: Physicochemical properties of the heterocycles

Compound	MW (g/mol)	HB_d	Hb_a	RB	LogD (7.4)	PSA (Å²)	pKa	$K_{liver:blood}$
Drug like[a]	< 500	≤ 5	≤ 5	≤ 10	≤ 5	≤ 140		
1271	270	1	2	4	2.8	55	10.02	7.74
1210	209	3	3	1	2.0	50	11.64	24.83
1270	300	1	2	5	3.6	42	13.49	17.11
1269	333	2	2	5	4.3	58	11.52/13.61	12.24
1214	319	2	2	4	4.3	58	10.59/11.63	10.33
1396	225	1	1	1	3.7	26	/	25.68
1365	330	1	2	4	4.8	42	10.87	7.32
1350	330	1	2	4	5.2	42	10.70	7.25
1352	334	1	2	4	4.8	55	10.01	7.43
1213	320	1	2	4	4.4	55	10.33	6.99
1354	366	1	3	4	5.0	51	10.49	9.14
1367	350	1	2	4	5.7	42	10.05	8.06
1398	319	1	1	4	4.7	42	10.60	7.67
1349	338	1	2	5	5.1	42	13.48	16.73
1399	335	1	1	4	5.5	29	10.74	7.39
1211	286	1	2	4	3.7	42	10.50	10.63
1348	350	1	2	4	5.7	42	10.49	8.74

[a] (Lipinski et al., 2001)

Abbreviations: MW molecular weight; HB_d hydrogen bond donor; HB_a hydrogen bond acceptor; RB rotatable bond; LogD distribution-coefficient; PSA polar surface area; pKa acid dissociation constant; $K_{liver:blood}$ liver-to-blood partition coefficient.

Table 2 Km and Km corrected for the unbound fraction in hepatocytes or microsomes for the metabolism of compound **1210** in rat liver microsomes and suspended rat hepatocytes along with calculated $Kp_{u,u}$ in suspended rat hepatocytes.

	Model system	
	Rat liver microsoms	**Suspended rat hepatocytes**
Km (µM)	38.33	7.80
Km x f_u (µM)	33.73	7.02
$Kp_{u,u}$		4.77

Abbreviations: RLM rat liver microsomes; SRH suspended rat hepatocytes; Km Michaelis Menten constant; f_u unbound fraction; $Kp_{u,u}$ ratio of the intracellular to extracellular unbound concentration.

805 **Table 3** *In vivo* prediction for hepatic clearance and extraction ratio (ER).

Compound	$Cl_{H,met}$ (ml/min/kg bodyweight)	$Cl_{H,uptake}$ (ml/min/kg bodyweight)	Cl_H (ml/min/kg bodyweight)	ER	Class
1271	4.6	18.0	5.4	0.19	P
1210	23.0	26.4	23.1	0.82	E
1270	12.6	23.8	12.0	0.42	I
1269	4.1	22.6	4.7	0.16	P
1214	17.3	25.6	16.0	0.56	I
1396	8.4	18.9	13.8	0.49	I
1365	3.0	6.1	2.1	0.08	P
1350	0.2	7.0	0.3	0.01	P
1352	1.2	4.2	1.6	0.06	P
1213	1.7	20.3	2.7	0.10	P
1354	0.3	5.0	0.5	0.02	P
1367	1.5	2.2	1.1	0.04	P
1398	0.8	11.2	0.8	0.03	P
1349	4.7	23.2	5.8	0.21	P
1399	0.6	15.6	0.9	0.03	P
1211	0.2	8.8	0.2	0.01	P
1348	0.5	7.8	0.6	0.02	P

806 Abbreviations: $Cl_{H,met}$ predicted *in vivo* clearance based on metabolism; $Cl_{H,uptake}$ predicted *in vivo*
807 clearance based on uptake; Cl_H predicted *in vivo* clearance based on uptake and metabolism; ER
808 extraction ratio; P poor clearance; I intermediate clearance; E extensive clearance.

809

810

Table 4 Classification of the heterocycles in the BCS and BDDCS

Compound	Solubility	Permeability Class	BCS Class	Metabolism (ER)	BDDCS Class
1271	I	H	I/II	P	III/IV
1210	H	H	I	E	I
1270	P	H	II	I	II/IV
1269	P	H	II	P	IV
1214	P	H	II	I	II/IV
1396	I	H	I/II	I	I-IV
1365	P	H	II	P	IV
1350	P	H	II	P	IV
1352	P	H	II	P	IV
1213	P	H	II	P	IV
1354	P	H	II	P	IV
1367	P	H	II	P	IV
1398	P	H	II	P	IV
1349	P	I	II/IV	P	IV
1399	P	I	II/IV	P	IV
1211	P	I	II/IV	P	IV
1348	P	I	II/IV	P	IV

Solubility based on threshold values: high solubility (H) > 500 mg/250 ml, intermediate solubility (I) 10 mg/250ml < x < 500 mg/250ml or poor solubility (P) < 10 mg/250 ml

Abbreviations: BCS biopharmaceutics classification system; BDDCS biopharmaceutics drug disposition classification system; USP United States Pharmacopeia. PI practically insoluble, VSS very slightly soluble, SS, slightly soluble